JOURNAL OF GEOPHYSICAL RESEARCH, VOL. 97, NO. B6, PAGES 8749–8764, JUNE 10, 1992

The Structure of the Core-Mantle Boundary From Diffracted Waves

MICHAEL E. WYSESSION,[1] EMILE A. OKAL, AND CRAIG R. BINA

Department of Geological Sciences, Northwestern University, Evanston, Illinois

Diffracted *P* and *S* waves (*Pd*, *Sd*) traveling around the core-mantle boundary (CMB) of the Earth give us information about the velocity structure and therefore the thermochemistry of D″, the base of the Earth's mantle. By examining *Pd* and *Sd* arrivals we determined the apparent ray parameter for different regions at the base of the mantle. By comparing the data slownesses to those found from reflectivity synthetic seismograms we were able to quantify D″ average velocities. Using these averaged velocities with a thermochemical modeling of lower mantle minerals using a Birch-Murnaghan equation of state, we have been able to make chemical and physical inferences as to the causes of lateral variations at the CMB. Examinations found significant lateral heterogeneity at the base of the mantle, amounting to ≈ 4% for both *P* and *S* velocities. These velocities did not always vary in parallel, and the Poisson ratio varied regionally by almost 6%. The most unusual region of the CMB found was under Indonesia, where velocities 3% slower than the preliminary reference Earth models were found adjacent to a region of faster than average velocities. These regions currently correspond to areas of core upwelling and downwelling (respectively) found by Voorhies (1986), which if mostly held in place by core-mantle coupling might cause a flux of heat and iron into the mantle, making the anomaly both thermally and chemically derived. At the CMB under the northern Pacific rim the fastest shear velocities were found, but the same region yielded slower than average *P* velocities. While the presence of fast shear velocities here would support the idea that we are seeing the cold dregs of mantle convection, perhaps continuing down from the North Pacific subduction zones, the presence of slow *P* velocities suggests additional complications. Our thermochemical modeling suggests that the D″ Poisson ratio is very sensitive to variations in the silicate/oxide ratio and that a decrease in the amount of perovskite relative to magnesiowüstite may play an important role in this region.

INTRODUCTION

The core-mantle boundary (CMB) is a very dynamic region, most likely as diverse and heterogeneous as the surface of the Earth. D″, so named by *Bullen* [1949], may be both a thermal and chemical boundary layer between the convecting crystalline mantle and the liquid iron core and may vary laterally much the same way the top 100 km of the Earth does. An understanding of this variation is vital to understanding the important processes that occur within the Earth (mantle convection, hot spot plume generation, core cooling, generation of the magnetic field, and reactions between the core and mantle) the same way that the identification of lateral variation at the surface was the key to understanding plate tectonics.

Our aim in this paper is to map out the lateral heterogeneity that exists within D″ in order to help facilitate attempts to understand the dynamics of this region. The method we present here involves modeling *P* and *S* waves that diffract around the CMB with reflectivity synthetic seismograms. These waves travel within D″ for great distances and are therefore the best seismic phases for examining long-wavelength CMB features. While our coverage of the CMB is far from complete (due to our study's stringent requirements for earthquake and station distributions), the resulting views that we do get of this unusual region suggest that it is dynamically active. The seismic velocities vary at levels more similar to those of the Earth's surface than for the rest of the lower mantle.

In previous studies, *Wysession and Okal* [1988, 1989] looked at the variations of CMB diffracted *S* and *P* waves, respectively. While both studies used normal mode summation to model the diffracted waves, the difficulties in attaining high frequencies with the normal modes, and in particular the spheroidal modes, limited our investigations not only to longer periods but to different frequency ranges for *P* and *S*. The use of the reflectivity synthetics in this study allows us to quantify our results relative to a reference Earth model and to quantify the differences between the *P* and *S* variations. In addition, we can then take the quantified D″ variations and attempt to make some physical interpretations using a simple thermochemical model. While we feel that neither seismology nor mineral physics are at such an advanced stage that D″ temperatures and compositions can be interpreted directly from seismic results, such modeling may represent the direction that geophysics will be taking.

The use of diffracted waves has long been established as a significant method for examining the base of the mantle because of the long distances that the waves can travel along the CMB and still be identified at the surface: in this study up to 60° for diffracted *P* (*Pd*) and 50° for diffracted *S* (*Sd*). Their identification is facilitated by being the first *P* and *SH* phases to arrive in the surface shadow zone of the core, where there are no direct geometrical phases, as is shown for *P* waves in Figure 1. In principle, *Pd* and *Sd* are simply extensions of Huygens' diffracted wave theory, with every point on the wave front being the site of an expanding spherical wavelet, though in reality the interaction of these waves with the Earth's CMB has made them difficult to model and many synthetic seismogram techniques are inadequate. Diffracted wave studies have involved both travel times and amplitudes, and though we will concentrate on the arrival times through the use of the ray parameter, we refer the use of the amplitudes to look at D″ attenuation to *Mondt* [1977], *Doornbos and Mondt* [1979*a*], and *Mula* [1981].

The ray parameter (slowness) of a profile of successive diffracted waves is an indication of the average D″ velocities along an azimuthal path across the CMB. The ray parameter p is determined by $p = dT/d\Delta = R_{CMB}/V_{CMB}$, where T is the travel time of arrival, Δ is the distance from the earthquake, R_{CMB} is the radius of the CMB, and V_{CMB} is the apparent velocity at the CMB. While at in-

[1]Now at Department of Earth and Planetary Sciences, Washington University, St. Louis, Missouri.

Paper number 92JB00511.
0148-0227/92/92JB-00511$05.00

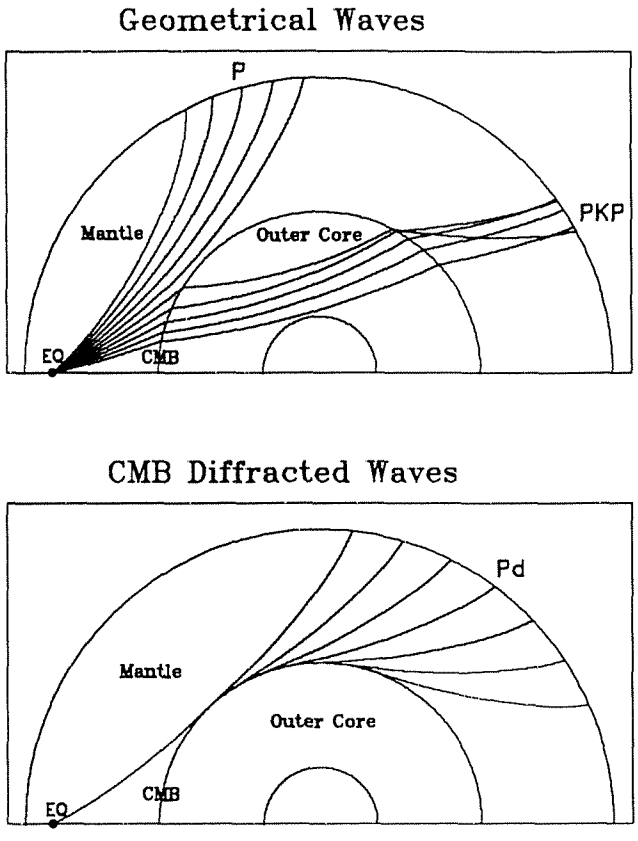

Fig. 1. A demonstration of the difference between geometrical waves (obeying Snell's Law) and diffracted waves. (Top) Ray tracing for *P* waves within the Earth, showing the shadow zone that exists between the *P* and *PKP* arrivals. (Bottom) Diffracted *P* waves (*Pd*) that travel along the core-mantle boundary and leak back to the surface, arriving within the shadow zone and beyond.

finite frequency the diffracted ray parameter should be linear, in actuality, V_{CMB} cannot be taken as the actual velocity at the base of the mantle because of several nonlinear effects. The complications that the diffracted waveforms undergo as they propagate around the CMB have been discussed by many papers including *Alexander and Phinney* [1966], *Chapman and Phinney* [1972], *Mula and Müller* [1980], and *Wysession and Okal* [1988, 1989], but the complications can be summarized as follows: (1) for a D" model featuring a non-zero velocity gradient, dispersion of the diffracted ray will occur with different frequencies traveling through regions of different velocities; (2) as the ray propagates along the CMB, its amplitude decreases due to diffraction back into the mantle; (3) energy will leak into the core for *Pd* and for *Sd* if there is nonzero rigidity at the top of the core; and (4) anelastic attenuation further reduces the high-frequency components of the signal. It is very important, therefore, that the apparent slownesses be interpreted through comparison with synthetic seismograms that take into account the frequency effects and, in particular, the exact geometry of the stations.

The arbitrariness of the apparent ray parameter is further enhanced by the manner in which it is measured. Three techniques have been utilized in diffracted wave studies: picking first motions, picking the times of the first peaks, and using a multi-waveform cross-correlation, and all three give different values for the same profile of stations.

Studies looking at the diffracted wave apparent slownesses have arrived at a wide assortment of values, though the published scatter for *Sd* has been greater than for *Pd*. For *Sd* some of the apparent ray parameters (in seconds per degree) have been 8.9 [*Cleary*, 1969], 8.94 [*Hales and Roberts*, 1970], 8.68 [*Bolt et al.*, 1970], 8.40 and 9.48 [*Bolt and Niazi*, 1984], 8.29-8.96 [*Mondt*, 1977], 8.53 (averaged [*Doornbos and Mondt*, 1979*b*]), 8.37-8.44 [*Okal and Geller*, 1979], and 8.23-8.66 [*Mula and Müller*, 1980]. Published *Pd* slownesses include 4.41, 4.56, 4.63 [*Espinoza*, 1967], 4.53 [*Sacks*, 1967], 4.55-4.60 [*Bolt*, 1970], 4.51-4.64 [*Mondt*, 1977], 4.55 (averaged, [*Doornbos and Mondt*, 1979*b*]), 4.27-4.64 [*Mula and Müller*, 1980], and 4.34-4.72 from International Seismological Centre (ISC) data and 4.37-4.51 from Swedish array data [*Båth*, 1986]. The scatter of these slownesses far exceeds the lateral heterogeneity that we have found and is testimony to the complications of determining the ray parameters of core diffracted waves.

DATA AND PROCEDURES

A total of 132 *Pd* arrivals from 13 large earthquakes and 71 *Sd* arrivals from 10 large earthquakes recorded on long-period World-Wide Standard Seismograph Network (WWSSN) and Canadian seismometers (as well as the Palisades Press-Ewing) were used for our study. This gave us 20 azimuthally independent *Pd* profiles and 12 *Sd* profiles. While the WWSSN and Canadian instruments have a more limited response than current broadband seismometers, the extensive network of similar instruments that flourished during the 1960s and 1970s allows us to find many profiles where several stations are along the same azimuth from a large earthquake. This density of coverage has not yet been attained by the digital broadband networks.

The records were digitized, interpolated at 0.5-s intervals using a cubic polynomial scheme, and, in the case of *Sd*, rotated into their transverse components to model the diffracted *SH* energy. This is done because diffracted *SV* decays quickly with distance (due to a conversion to *P* energy into the core as phases like *SdKS* or *SPdKS* [*Choy*, 1977]). Observations of *SVd* far into the shadow zone, like that seen by *Vinnik et al.* [1989] at 117°, are rare. The hypocenters and focal mechanisms of the earthquakes used are in Table 1, and the path profiles (including the split profiles for the Tonga to Mid-East paths) are listed in Table 2.

Calculated for the Preliminary Reference Earth Model (PREM) structure of *Dziewonski and Anderson* [1981], the first diffracted arrivals (the edge of the shadow zone) from a surface earthquake are at $\Delta = 98.4°$ for *Pd* and $\Delta = 102.7°$ for *Sd*. For an earthquake at a depth of 600 km these distances are $\Delta = 96.2°$ for *Pd* and $\Delta = 100.4°$ for *Sd*. As a consequence we tried to avoid using any arrivals closer than 100°, only twice using *Sd* arrivals that contained mostly undiffracted *SH* energy. The diffracted energy decays quickly along the CMB, but we found as appropriate for our study four *Sd* arrivals and seven *Pd* arrivals recorded beyond 150°, making the range of the CMB sampled by a given profile to be as great or greater than 50°, or 3000 km. It was always our attempt to get as many arrivals with as wide a distance range as possible for each path used, and as a consequence, our slownesses are averaged over very long wavelengths. While other techniques have detected inhomogeneity in D" on scales significantly smaller than 3000 km, this averaging was propitious due to the more robust determination of the ray parameter using a broader distance range. The ranges of the epicentral distances are given in Table 2. It is convenient to think of the diffracted rays as traveling as a narrow pencil across the CMB, but we are actually sampling material along a broad swath that is frequency dependent.

TABLE 1. Earthquakes Used for the *Pd* and *Sd* Profiles

Type	Location	Date	Origin Time, UT	Depth, km	Latitude °N	Longitude °E	m_b	Strike	Dip	Slip	Source
P	Taiwan	Feb. 13, 1963	08 50:05.0	53	24.41	122.09	6.2	79	61	90	1
P	Peru	Aug. 15, 1963	17 25:11.0	593	-13.78	-69.26	6.0	52	46	-56	2
P	Brazil	Nov. 9, 1963	21 15:30.0	576	-8.83	-71.67	5.9	163	48	-97	3
S	New Guinea	April 24, 1964	05 56:09.8	99	-5.07	144.20	6.3	183	80	-90	4
P	Sandwich Islands	Sept. 14, 1966	23 18:41.9	27	-60.33	-27.25	5.9	80	52	90	5
S	Loyalty Islands	Oct. 7, 1966	15 55:11.3	165	-21.59	170.56	6.0	107	70	21	4
P	Sumatra	May 21, 1967	18 45:13.2	184	-0.96	101.39	6.2	158	70	95	6
P	Sumatra	Aug. 21, 1967	07 33:01.6	40	3.72	95.74	6.1	113	78	90	7
P,S	Tonga	Oct. 9, 1967	17 21:46.0	605	-21.10	-179.20	6.2	54	85	-83	4
P	Nicaragua	Oct. 15, 1967	08 00:52.6	181	11.91	-85.98	6.2	148	73	97	4
P	Kermadec	July 25, 1968	07 23:02.0	17	-30.97	-178.13	6.5	12	60	90	8
P	Molucca Sea	Aug. 10, 1968	02 07:00.0	1	1.38	126.24	6.3	172	46	79	9
P,S	Tonga	Feb. 10, 1969	22 58:03.3	635	-22.75	178.76	6.0	96	86	-65	9
S	Burma	July 29, 1970	10 16:20.4	68	26.02	95.37	6.4	197	60	165	10
S	Kuril Islands	Jan. 29, 1971	21 58:05.4	515	51.69	150.97	6.0	35	71	-90	5
S	Tonga	Nov. 20, 1971	07 27:59.5	533	-23.45	-179.88	6.0	160	75	100	5
P	Kermadec	March 30, 1972	05 34:50.4	479	-25.69	179.58	6.1	179	82	55	9
P	Northern Korea	Sept. 29, 1973	00 44:00.3	567	41.93	130.99	6.3	194	64	77	5
S	Tonga	Feb. 22, 1975	22 04:33.5	333	-24.98	-178.88	6.1	35	87	-143	5
S	Honshu	June 29, 1975	10 37:40.6	549	38.79	130.09	6.1	222	78	120	5
S	Honshu	March 9, 1977	14 27:53.6	579	41.61	130.88	5.9	194	75	76	11

References for focal mechanisms: (1) *Katsumata and Sykes* [1969]; (2) *Chandra* [1970]; (3) *Berckhemer and Jacob* [1968]; (4) *Isacks and Molnar* [1971]; (5) this study; (6) *Fitch and Molnar* [1970]; (7) *Fitch* [1970]; (8) *Johnson and Molnar* [1972]. It is worth noting that they have mixed up the azimuth and plunge of the two nodal plane poles in their Table 3, as evidenced by the inclusion of a picture of the focal mechanism showing the station polarities. A correct listing of the event appears in *Denham* [1977]; (9) *Mula* [1981]; (10) *Tandon and Srivastava* [1975]; (11) *Giardini* [1984].

It is very important, however, that a narrow range of takeoff azimuths be accepted for the inclusion of arrivals in a given path profile. *Cormier* [1989] has shown that contamination of *S* rays by slab-diffracted energy can cause a difference in arrival times of several seconds for rays leaving a subduction zone earthquake at different azimuths. In addition, rays at varying azimuths could accrue travel time differences due to their different downswing paths through the heterogeneous mantle. Most importantly, a narrow azimuthal range not only eliminates errors due to source effects and heterogeneity by studying essentially the same ray along its downswing path but also allows the waves to sample the same portions of the CMB so that the apparent ray parameter supplies information about one particular strip across D". The azimuthal windows used are shown in Table 2: the largest were 22° and 21° for *Pd* and *Sd*, respectively, and the average for both was 12°. Examples of our profiles of *Pd* are given in Figure 2, which shows the *Pd* profiles from the Tonga (October 9, 1967) earthquake to both North America (top) and the Mid-East (bottom). Note the clear surface reflected arrivals *pPd* and *sPd* as well as *Pd*. The complete data sets are plotted by *Wysession* [1991].

In order to retain large amounts of diffracted energy around the CMB the events used in this study were all large ($m_b > 5.9$). The source parameters were either taken from previous studies or calculated on the basis of first arrivals. We preferred to use deep events for several reasons. The low-velocity zone at the base of the lithosphere greatly attenuates *S* waves that pass through it, and rays from deeper events pass through this zone once instead of twice. Records from deep events are usually cleaner and less noisy, making the diffracted arrivals more distinct, but more importantly with deep events, *Pd* and *Sd* are also distinct from their surface reflections (*pPd*, *sPd*, *sSd*), simplifying the procedure of determining the slownesses.

Another requirement for the earthquake sources was that their radiation amplitudes be favorable for the azimuths along which the string of stations are located. These amplitudes, calculated using the formulation of *Kanamori and Stewart* [1976], are shown for the profiles in Table 2. The radiation amplitudes had means of 0.74 for the *Pd* profiles and 0.56 for *Sd* (the optimal relative amplitude is $R = 1$). In the few cases where the radiation amplitude was low, the profiles were only retained if they had very clear and simple signals.

Corrections to Data

In order to further equate the filtered data with the synthetics, corrections for upper mantle heterogeneity along the *Pd* and *Sd* upswings were added to the travel times based on the tomographic full mantle shear velocity model of *Woodhouse and Dziewonski* [1987]. The process involved tracing each diffracted ray's upswing mantle path through the tomographic model to calculate the predicted travel time delay and is described in more detail by *Wysession and Okal* [1988, 1989]. The difficulty here was to find a compatible means of comparison for both the *S* and *P* waves. We decided to use the *Woodhouse and Dziewonski* [1987] model for the *P* waves as well, adjusting the travel time delays according to $d(\ln \alpha)/d(\ln \beta) \approx 0.5$ [*Bina and Silver*, 1990]. Though the change in

TABLE 2. CMB Path Profile Data for *Pd* and *Sd*

Date	CMB Path Description	Number of Stations	Distance Range, deg	Azimuth Range, deg	Radiation Amplitude
	Pd Profiles				
Feb. 13, 1963	Taiwan to South America (1)	6	112-145	6-16	0.97
Feb. 13, 1963	Taiwan to South America (1)	5	100-147	20-31	0.95
Feb. 13, 1963	Taiwan to South America (1)	7	100-149	31-42	0.94
Aug. 15, 1963	Peru to South Asia	4	101-159	54-59	0.96
Nov. 9, 1963	Brazil to South Asia	7	100-145	50-62	0.71
Sept. 14, 1966	Sandwich Islands to North America	10	104-129	297-314	0.92
May 21, 1967	Sumatra to North America	6	100-144	24-35	0.88
Aug. 21, 1967	Sumatra to North America	5	120-136	27-33	0.89
Oct. 9, 1967	Tonga to North America	8	102-123	50-58	0.14
Oct. 9, 1967	Tonga to Mid-East (whole)	6	111-148	291-303	0.79
Oct. 9, 1967	Tonga to Mid-East (first part)	3	111-127	293-300	0.79
Oct. 9, 1967	Tonga to Mid-East(second Part)	4	127-148	292-303	0.79
Oct. 15, 1967	Nicaragua to South Asia	5	100-144	34-50	0.92
July 25, 1968	Kermadec to North America	6	109-128	56-62	0.57
July 25, 1968	Kermadec to Europe	6	113-157	12-23	0.77
July 25, 1968	Kermadec to Mid-East (whole)	8	116-161	280-296	1.00
July 25, 1968	Kermadec to Mid-East(first part)	4	116-132	287-292	1.00
July 25, 1968	Kermadec to Mid-East(second part)	5	132-161	280-296	1.00
Aug. 10, 1968	Molucca Sea to North America	7	107-157	25-37	0.97
Aug. 10, 1968	Molucca Sea to Europe	7	102-133	321-332	0.96
Feb. 10, 1969	Tonga to Mid-East (whole)	7	110-147	290-302	0.27
Feb. 10, 1969	Tonga to Mid-East (first part)	4	110-126	293-299	0.27
Feb. 10, 1969	Tonga to Mid-East(second part)	4	126-147	290-302	0.27
March 30, 1972	Kermadec to North America	6	105-121	55-63	0.79
March 30, 1972	Kermadec to Mid-East (whole)	8	99-148	287-297	0.45
March 30, 1972	Kermadec to Mid-East (first part)	5	99-121	291-296	0.44
March 30, 1972	Kermadec to Mid-East (second part)	5	120-148	287-297	0.45
Sept. 29, 1973	Northern Korea to South America	8	113-155	32-53	0.91
	Sd Profiles				
April 24, 1964	New Guinea to Europe	5	109-137	330-340	0.83
Oct. 7, 1966	Loyalty Islands to Mid-East (whole)	6	103-139	292-300	0.48
Oct. 7, 1966	Loyalty Islands to Mid-East (first part)	4	103-119	295-300	0.46
Oct. 7, 1966	Loyalty Islands to Mid-East (second part)	4	111-139	292-300	0.48
Oct. 9, 1967	Tonga to North America	6	102-130	45-54	0.92
Oct. 9, 1967	Tonga to Mid-East	4	98-133	291-294	0.46
Feb. 10, 1969	Tonga to North America	8	104-132	46-58	0.57
Feb. 10, 1969	Tonga to Mid-East (whole)	7	110-150	290-302	0.59
Feb. 10, 1969	Tonga to Mid-East (first part)	3	110-126	293-299	0.59
Feb. 10, 1969	Tonga to Mid-East(second Part)	5	126-150	290-302	0.59
July 29, 1970	Burma to North America	7	112-123	354-365	0.23
Jan. 29, 1971	Kuril Islands to Americas	5	112-133	49-62	0.75
Nov. 20, 1971	Tonga to Mid-East (whole)	6	106-148	274-293	0.52
Nov. 20, 1971	Tonga to Mid-East (first part)	3	106-121	274-293	0.52
Nov. 20, 1971	Tonga to Mid-East (second part)	4	121-148	288-292	0.58
Feb. 22, 1975	Tonga to North America	6	103-132	49-58	0.29
June 29, 1975	Honshu to Americas	6	101-144	29-49	0.50
March 9, 1977	Honshu to Americas	5	98-150	22-38	0.71

the ray parameter that resulted from these travel time corrections was usually insignificant, they could on occasion be more important, having maxima of 0.7% for both the *Pd* and *Sd* profiles. We also calculated *Sd* corrections using the upper mantle shear model of *Tanimoto* [1987] and *Pd* corrections using the station corrections of *Dziewonski and Anderson* [1983], and in both cases the differences from the *Woodhouse and Dziewonski* [1987] corrections caused insignificant differences in the ray parameters. While it may be in poor taste philosophically to use a shear wave model to make *P* wave corrections, especially when we will later look at differences between *P* and *S* velocities in D", it is not inappropriate. The velocity variations found in D" are an order of magnitude greater than the mantle heterogeneity corrections to the ray parameters, making second-order differences between models less of a problem for the current study. It is also interesting to note that in most cases, for both *Sd* and *Pd*, the travel time corrections improved the quality of the correlation coefficient of the slowness determination, implying that it was removing mantle "noise" from a more coherent D" signal.

We also made corrections for ellipticity to the diffracted data, using the tables of *Jeffreys and Bullen* [1970]. For *Pd* the corrections ranged from -1.15 s to +1.07 s and often differed by more than 1 s for arrivals along a single profile. For *Sd* the range was from -0.26 s to +1.28 s. These corrections affected the slownesses

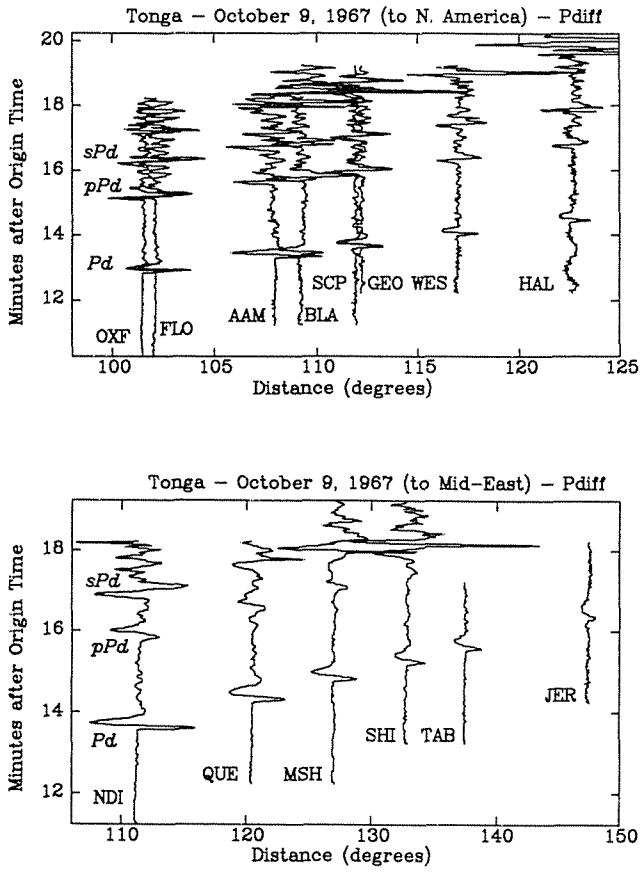

Fig. 2. The diffracted P arrivals at stations in (top) North America and (bottom) the Mid-East from the earthquake in Tonga on October 9, 1967. Note that time scales are slightly different.

by the same order as the mantle upswing corrections: they were usually not important, but were as great as 0.9% and 0.6% for the *Pd* and *Sd* profiles, respectively.

Slowness Determination

There are three methods of determining the linear ray parameter through the diffracted arrivals, as was addressed by *Wysession and Okal* [1989]. Picking first motions, as was used most recently by *Bolt and Niazi* [1984], was found to be the least reliable method. The error in choosing an onset time for the diffracted waves, which are usually of small amplitude and occasionally emergent, could be of the order of several seconds. Picking the pulse maxima of the first peaks was used by *Mondt* [1977] and *Mula and Müller* [1980] and has the advantage of yielding easily chosen times. Multiwaveform cross correlations of the windowed pulses were used by *Okal and Geller* [1979] and *Wysession and Okal* [1988] and were the least sensitive to signal noise. As with *Wysession and Okal* [1989], we will determine the slownesses (for the data and synthetics) using both the peak maxima (PM) and multiwaveform cross correlation (XC) methods, and we will determine final comparisons with the averages of the two. Both of these methods for determining the ray parameter are affected by the changing frequency contents of the arrivals and will therefore be different, but the effect should be the same for both data and synthetics. Examples of these two methods are shown for the Kermadec (March 30, 1972) to Mid-East *Pd* profile in Figures 3 and 4.

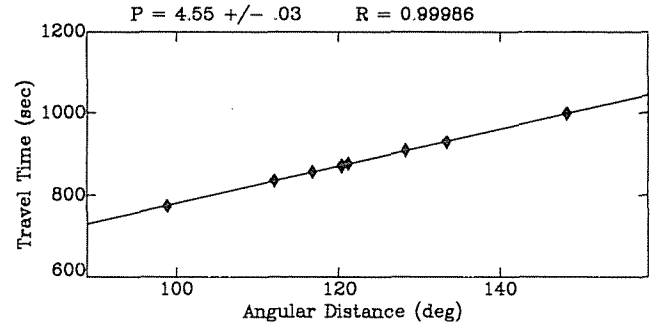

Fig. 3. An example of the linear regression used to determine the apparent *Pd* slowness using the pulse maxima approach, shown here for the Kermadec (March 30, 1972) to Mid-East profile. The slowness is the best fit line through the arrival peak travel times, and the error ±0.03 s/deg) is found assuming errors in the arrival times of ±1 s.

Reflectivity Synthetic Seismograms

Our previous normal mode studies were not able to take advantage of a large portion of the seismic energy recorded on the WWSSN instruments (at periods less than $T = 20$ s), so to allow for this as well as a comparison between the *Pd* and *Sd* results we modeled the data using reflectivity synthetic seismograms at periods $T \geq 4$ s. They were generated using a computer program adapted from the work of B. L. N. Kennett. This process involves a numerical integration over frequency and slowness for the propagation of elastic energy from a double-couple source where the integrand is specified in terms of the reflection and transmission coefficients for a flat, stratified Earth. It has been previously used to model core diffracted waves by *Mula and Müller* [1980] and *Mula* [1981].

The synthetics were calculated using appropriate focal parameters, and delta functions were used as sources, with the resulting

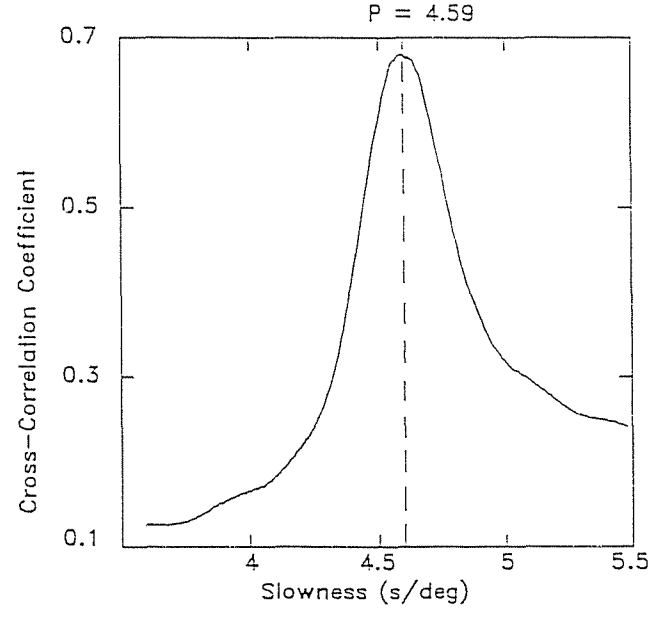

Fig. 4. An example of the multiwaveform cross-correlation technique used to determine the *Pd* apparent slowness for the Kermadec (March 30, 1972) to Mid-East profile. The best value of the slowness is the peak of the curve.

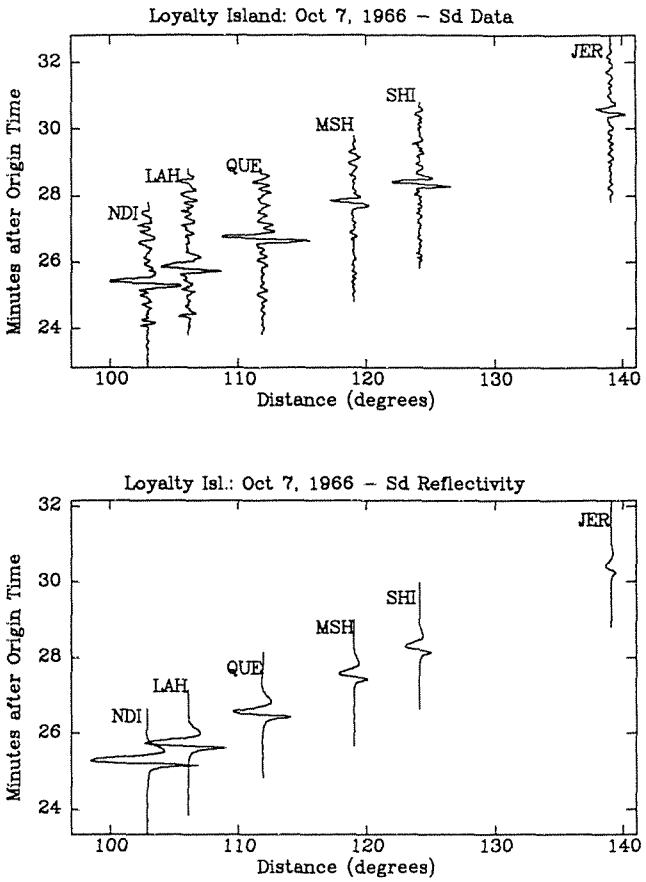

Fig. 5. An example of the reflectivity synthetic seismograms, shown here modeling the diffracted *S* arrivals from the Loyalty Island (October 7, 1966) earthquake. Data are shown at the top, and synthetics are shown at the bottom. Note that time scales are slightly different.

ground motions then convolved with the proper WWSSN instrument responses. Examples of the synthetics are given in Figure 5, which shows the reflectivity synthetics for the *Sd* profile from Loyalty Island (October 7, 1966) to the Mid-East, with the data included for comparison. In order to facilitate the comparisons between *P* and *S* velocity variations the *Pd* and *Sd* data were handled and processed in similar manners. All records were filtered to retain periods above $T \geq 4$ s to give them the same frequency contents as the reflectivity synthetics, ellipticity corrections were made to the *Pd* and *Sd* data, and slownesses were determined using the PM and XC methods.

RAY PARAMETER DETERMINATIONS

Synthetic Slownesses

The results of the slowness determinations for the data and reflectivity synthetics are given in Table 3. Standard errors (σ) are given, and are calculated for the linear regression through the peak maxima assuming ±1 s errors in the arrival times. They are a function of the number of stations and distance ranges of the profiles (more stations or a longer distance range yields a smaller σ) but not the quality of the waveforms. The quality of the full waveforms (e.g., signal-to-noise ratio, signal contamination) is manifested in the cross correlograms, and though there was not a straightforward way to measure the standard error from these, all of the profiles retained for the study yielded sharp unitary cross-correlogram peaks. The mean values for the standard deviations of the profile slownesses were $\sigma = 0.046$ s/deg for *Pd* and $\sigma = 0.051$ s/deg for *Sd*.

We can draw some useful conclusions by looking at the data set as a whole. In general, the data had slownesses that implied slightly slower velocities than inferred from the PREM reflectivity synthetics. We found mean profile slownesses for the *Pd* data of 4.587 s/deg (XC) and 4.552 s/deg (PM), and for the *Pd* synthetics of 4.551 s/deg (XC) and 4.523 s/deg (PM). For *Sd* our profiles yielded average slownesses for the data of 8.487 s/deg (XC) and 8.483 s/deg (PM), and for the PREM synthetics of 8.473 s/deg (XC) and 8.437 s/deg (PM). As a whole, the *Pd* data slownesses were 0.033 s/deg (0.7%) higher than for the PREM synthetics, and the *Sd* data slownesses were also high by 0.030 s/deg (0.35%), implying average D" velocities slightly but not significantly slower than for PREM.

The difference between the XC and PM slownesses, discussed earlier, is found in both the data and synthetics. The difference between the *Pd* mean XC and PM data slownesses is 0.035 s/deg, and between the XC and PM synthetics is 0.029 s/deg (XC is higher). This trend did not appear in the *Sd* data, however, which have nearly identical XC and PM means even though the *Sd* synthetics predict a 0.036 s/deg difference between the two. This could be related to previous observations that the high frequency content decays less rapidly for *S* than for *P*, which loses energy quickly into the core as *PdKP*.

The synthetic apparent ray parameters display a noticeable variability. This is expected and is the reason why the synthetics were generated in the exact geometries of the various profiles. The number of stations, the distance separations between them, and the type of recording instruments used will all affect the resulting slownesses, as can be seen in Table 3. Especially prominent are the differences between slownesses determined on WWSSN 30/100 and 15/100 instruments, as documented by the four events in 1963-1964 when the WWSSN was still operating in the old $T_p = 30$ s configuration. The five *Pd* profiles extracted from these 30/100 instruments yielded synthetic slownesses averaging 4.584 s/deg (XC) and 4.544 s/deg (PM), significantly higher than for the 15/100 slownesses which averaged 4.544 s/deg (XC) and 4.518 s/deg (PM). The case was similar for the one *Sd* profile with 30/100 instruments (the New Guinea earthquake of April 24, 1964).

Data Slownesses

The variation in the data slownesses left after comparisons with the synthetics is interpreted as lateral heterogeneity in D" velocities. The range of *Pd* slowness residuals (data slownesses minus the slownesses of the synthetics) is 0.31 s/deg (6.8%), and the range for *Sd* slowness residuals was 0.72 s/deg (8.5%). A more statistically reliable determination of the ray parameter variation is by looking at the standard deviations of the slowness residuals. For *Pd* this is 0.071 s/deg, corresponding to 3.1% variation, and for *Sd* the standard deviation is 0.18 s/deg, corresponding to a 4.3% variation. We will base following conclusions, however, on the path-averaged values of the inferred D" velocities.

Converting Slownesses to Velocities

Once the data slownesses are determined relative to the synthetics, we can average the results for profiles that travel the same CMB paths. What we have is a measure of the percentage difference of the diffracted wave ray parameter in different parts of D" relative to a PREM D". What we would like is a measure of the

TABLE 3. Apparent Slownesses for the Data and Reflectivity Synthetics

Date	CMB Path Description	Slowness, s/deg				σ, s/deg
		Data		Synthetics		
		XC	PM	XC	PM	
	Pd Profiles					
Feb. 13, 1963	Taiwan to South America (1)	4.55	4.50	4.59	4.54	0.03
Feb. 13, 1963	Taiwan to South America (1)	4.64	4.56	4.58	4.54	0.05
Feb. 13, 1963	Taiwan to South America (1)	4.62	4.58	4.59	4.54	0.02
Aug. 15, 1963	Peru to South Asia	4.64	4.69	4.59	4.55	0.05
Nov. 9, 1963	Brazil to South Asia	4.62	4.55	4.57	4.55	0.03
Sept. 14, 1966	Sandwich Islands to North America	4.60	4.51	4.54	4.51	0.04
May 21, 1967	Sumatra to North America	4.61	4.60	4.56	4.51	0.03
Aug. 21, 1967	Sumatra to North America	4.60	4.55	4.55	4.51	0.05
Oct. 9, 1967	Tonga to North America	4.55	4.57	4.52	4.50	0.03
Oct. 9, 1967	Tonga to Mid-East (whole)	4.54	4.51	4.57	4.52	0.03
Oct. 9, 1967	Tonga to Mid-East (first part)	4.67	4.63	4.52	4.53	0.09
Oct. 9, 1967	Tonga to Mid-East(second Part)	4.47	4.50	4.56	4.51	0.07
Oct. 15, 1967	Nicaragua to South Asia	4.61	4.56	4.56	4.52	0.05
July 25, 1968	Kermadec to North America	4.51	4.53	4.51	4.49	0.07
July 25, 1968	Kermadec to Europe	4.55	4.54	4.54	4.52	0.03
July 25, 1968	Kermadec to Mid-East (whole)	4.61	4.53	4.54	4.52	0.02
July 25, 1968	Kermadec to Mid-East(first part)	4.80	4.77	4.52	4.53	0.08
July 25, 1968	Kermadec to Mid-East(second part)	4.51	4.45	4.53	4.52	0.04
Aug. 10, 1968	Molucca Sea to North America	4.57	4.53	4.54	4.50	0.03
Aug. 10, 1968	Molucca Sea to Europe	4.51	4.44	4.51	4.50	0.04
Feb. 10, 1969	Tonga to Mid-East (whole)	4.54	4.54	4.57	4.52	0.03
Feb. 10, 1969	Tonga to Mid-East (first part)	4.70	4.69	4.52	4.54	0.09
Feb. 10, 1969	Tonga to Mid-East(second part)	4.52	4.56	4.57	4.51	0.07
March 30, 1972	Kermadec to North America	4.49	4.45	4.54	4.50	0.07
March 30, 1972	Kermadec to Mid-East (whole)	4.59	4.55	4.55	4.51	0.03
March 30, 1972	Kermadec to Mid-East (first part)	4.65	4.65	4.53	4.50	0.05
March 30, 1972	Kermadec to Mid-East (second part)	4.53	4.49	4.59	4.52	0.04
Sept. 29, 1973	Northern Korea to South America	4.64	4.62	4.57	4.52	0.03
	Sd Profiles					
April 24, 1964	New Guinea to Europe	8.53	8.52	8.50	8.45	0.05
Oct. 7, 1966	Loyalty Islands to Mid-East (whole)	8.48	8.50	8.47	8.44	0.03
Oct. 7, 1966	Loyalty Islands to Mid-East (first part)	8.93	9.01	8.45	8.44	0.08
Oct. 7, 1966	Loyalty Islands to Mid-East (second part)	8.34	8.33	8.46	8.44	0.05
Oct. 9, 1967	Tonga to North America	8.49	8.54	8.49	8.43	0.05
Oct. 9, 1967	Tonga to Mid-East	8.50	8.50	8.48	8.44	0.04
Feb. 10, 1969	Tonga to North America	8.32	8.28	8.47	8.44	0.05
Feb. 10, 1969	Tonga to Mid-East (whole)	8.46	8.46	8.48	8.44	0.03
Feb. 10, 1969	Tonga to Mid-East (first part)	8.81	8.79	8.47	8.45	0.09
Feb. 10, 1969	Tonga to Mid-East(second Part)	8.34	8.34	8.48	8.43	0.05
July 29, 1970	Burma to North America	8.48	8.43	8.46	8.43	0.10
Jan. 29, 1971	Kuril Islands to Americas	8.37	8.31	8.47	8.44	0.05
Nov. 20, 1971	Tonga to Mid-East (whole)	8.49	8.48	8.47	8.44	0.02
Nov. 20, 1971	Tonga to Mid-East (first part)	8.74	8.76	8.44	8.43	0.09
Nov. 20, 1971	Tonga to Mid-East (second part)	8.39	8.37	8.48	8.44	0.04
Feb. 22, 1975	Tonga to North America	8.46	8.47	8.49	8.43	0.05
June 29, 1975	Honshu to Americas	8.36	8.34	8.48	8.43	0.03
March 9, 1977	Honshu to Americas	8.27	8.27	8.48	8.44	0.02

percentage difference of the average velocities in different parts of D" relative to the average velocity in PREM's D". The apparent slownesses can be easily converted into apparent velocities by definition, but the translation of these apparent velocities into actual D" velocities is very complicated. A determination of the radial structure of D" is beyond the scope of this study, though eventually broadband arrays may give enough frequency amplitude information to invert for D" radial velocities, much as is done in surface wave inversions.

It is possible, however, using the results of *Mula and Müller* [1980], to translate the apparent velocities into average velocities if a specific depth is determined for D". Using 12 different velocity models that varied essentially only in the bottom 190 km of the mantle, *Mula and Müller* [1980] generated reflectivity synthetic diffracted *Pd* waves and determined the apparent ray parameters, which gave them the apparent D" velocities. They found a striking linear correlation between these apparent velocities α_{app} and the *P* velocity averaged over the bottom 190 km of the mantle (α_{190}). Their conclusion was that if D" was assumed to be 190 km thick, then $\alpha_{190} \propto 0.83\alpha_{app}$ (km/s). A similar result for shear waves yielded $\beta_{190} = \propto 0.65\beta_{app}$. The frequency spectra of *S* and *P* waves are different, and while we would expect them to interact with the bot-

TABLE 4. D" Velocities Relative to PREM Averaged over 190 km and Inferred From the Apparent Slownesses of Diffracted P and S Wave Profiles

Number of Profiles	Path Description	CMB Region Sampled	ΔV_{190}
	Diffracted P		
1	Taiwan to the Eastern Americas	Arctic Ocean / northern Canada	+0.8%
3	Taiwan/Korea to the Western Americas	northwest North America	-1.0%
3	Indonesia to North America	North Pacific Rim	-0.9%
3	Tonga to North America	east central Pacific	-0.1%
1	Sandwich Islands to North America	northeast South America	-0.6%
3	South America to Europe/Asia	northeast Atlantic / Mediterranean	-1.0%
1	Tonga to Europe/Asia	northern Pacific	-0.3%
1	Indonesia to Europe	north central Asia	+0.6%
4	Tonga to Mid-East (whole)	Indonesia / Southeast Asia	-0.3%
4	Tonga to Mid-East (first part)	Indonesia	-3.2%
4	Tonga to Mid-East (second part)	Southeast Asia	+0.7%
	Diffracted S		
1	Burma to North America	Artic Ocean	-0.1%
1	Indonesia to Europe	north central Asia	-0.4%
3	Japan/Kuriles to Americas	northwest North America	+1.0%
3	Tonga to North America	east central Pacific	+0.5%
4	Tonga to Mid-East (whole)	Indonesia / Southeast Asia	-0.2%
3	Tonga to Mid-East (first part)	Indonesia	-3.1%
3	Tonga to Mid-East (second part)	Southeast Asia	+0.8%

tom of the mantle in different ways, it is our hope that the empirical relationships of *Mula and Müller* [1980] will account for much of this. In our discussions of average D" velocities we will use these relationships to convert apparent velocities into D" average velocities with the arbitrary assumption that D" is 190 km thick, though it should be understood that the average velocities must increase if D" is thinner and must decrease if D" is thicker.

SEISMIC RESULTS

The variations in path-averaged velocities, determined by differences between the data slownesses and PREM synthetics, are shown in Table 4. The actual range in individual apparent ray parameters was large: 4.44-4.80 s/deg for *Pd* and 8.27-9.01 s/deg for *Sd*. When compared with the synthetics and averaged by region, the lateral variations were more moderate but still amounted to several percent for both *P* and *S* velocities. The path-averaged inferred velocities are shown in Figures 6 and 7. Solid circles represent earthquake locations, and the solid lines extending from them are the mean azimuths for each profile. The shaded regions show those parts of the CMB that are represented by the ray parameters, though the widths are only drawn schematically. As can be seen in Table 4, PREM does a fairly good job of serving as a reference model for the diffracted data, though there are roughly twice as many CMB regions that are slightly slower than PREM than are faster than PREM. It is not uncommon for a region to be faster or slower by about 1%, with the significant exception being under Indonesia. The regions we examined, including the path through Indonesia, displayed a total of 4.0% and 4.1% lateral variation in α_{190} and β_{190}, respectively, implying that the level of heterogeneity for *P* and *S* is approximately the same. In our regional discussion it is important to bear in mind that for the 1 s PREM velocities, α_{190} and β_{190} (over the 190 km at the base of the mantle) are 13.690 km/s and 7.264 km/s. For those paths which had both *P* and *S* coverage, the inferred values of α_{190} and β_{190} are shown in Table 5, along with the resulting Poisson ratios.

Certainly the most unusual region of the CMB that we found was underneath northern Indonesia and Southeast Asia, as sampled from the diffracted wave profiles from the Tonga/Kermadec region across the Mid-East to the Mediterranean. There was very good coverage along this profile, with as many as eight stations well separated with a total distance range of up to 49°, and this allowed us to examine the first and second halves of the path separately, both retaining high-quality profiles of several stations. The path profiles, when examined whole, showed no unusual velocities. Both α_{190} and β_{190} were nearly identical to those of PREM, with each being slightly slow (see Table 4). When separated, however, the second part showed slightly fast *P* and *S* velocities, but the first half had extremely slow velocities. We attempted to split up other profiles that had long distance ranges, and though in none of those cases did we find significant differences between the halves, their cross correlograms were not good enough to include in the study.

Along the first half of the Tonga to Mid-East path, sampling CMB under northern Indonesia, the apparent slowness was 3.8% slower than PREM for *P* waves and 4.7% slower for *S* waves. Again, using the assumptions above for a 190 km thick D", this would imply the velocity anomalies to be $\Delta\alpha_{190} = -3.2\%$ and $\Delta\beta_{190} = -3.1\%$ ($\alpha_{190} = 13.25$ km/s and $\beta_{190} = 7.04$ km/s). These are by far the lowest average D" velocities that we have yet found. The results are very robust, found nearly identically in profiles from four earthquakes for *Pd* and three earthquakes for *Sd*. What makes this even more unusual is that the second half of these profiles, under Southeast Asia, is unusually fast, relative to PREM. The implied velocity anomalies along this segment were $\Delta\alpha_{190} = +0.7\%$ and $\Delta\beta_{190} = +0.8\%$. This juxtaposition of slow and fast velocities also appears in tomographic studies that use nondiffracted arrivals, such as those of *Morelli and Dziewonski* [1987] (Model V3), *Tanimoto* [1987], and *Inoue et al.* [1990].

It is interesting to note that the *P* and *S* velocities do not always differ from PREM in the same way. *Wysession and Okal* [1988, 1989] found that the CMB region underneath Alaska and Canada, along the northern rim of the Pacific, had relatively fast *S* velocities

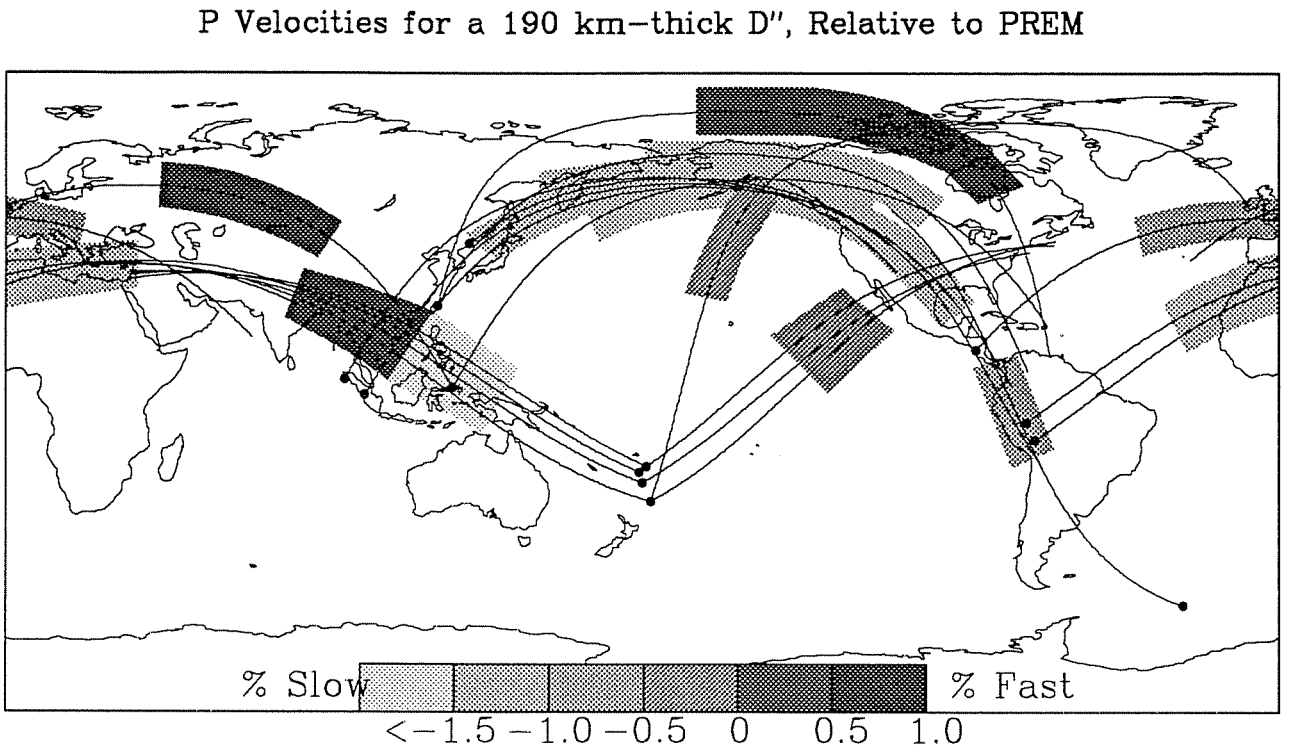

Fig. 6. Map of D" average *P* velocities relative to PREM [*Dziewonski and Anderson*, 1981], inferred from a comparison of *Pd* data and reflectivity synthetic seismogram ray parameters. Solid circles are earthquakes locations, the solid lines are the profile azimuths, and the shaded regions (with schematic widths) are the parts of the CMB sampled.

and relatively slow *P* velocities, and in quantifying this with the reflectivity synthetics we still found this to be true. The three *Sd* profiles from Japan and the Kurile Trench to the Americas had a velocity anomaly of $\Delta\beta_{190} = +1.0\%$, whereas for three similar profiles from Taiwan/Korea to the Americas (as well as three from Indonesia to North America) the *P* anomaly was $\Delta\alpha_{190} = -1.0\%$. In terms of the Poisson ratio ν this represents a -4% departure from PREM. The fast shear velocities occur in the same region where

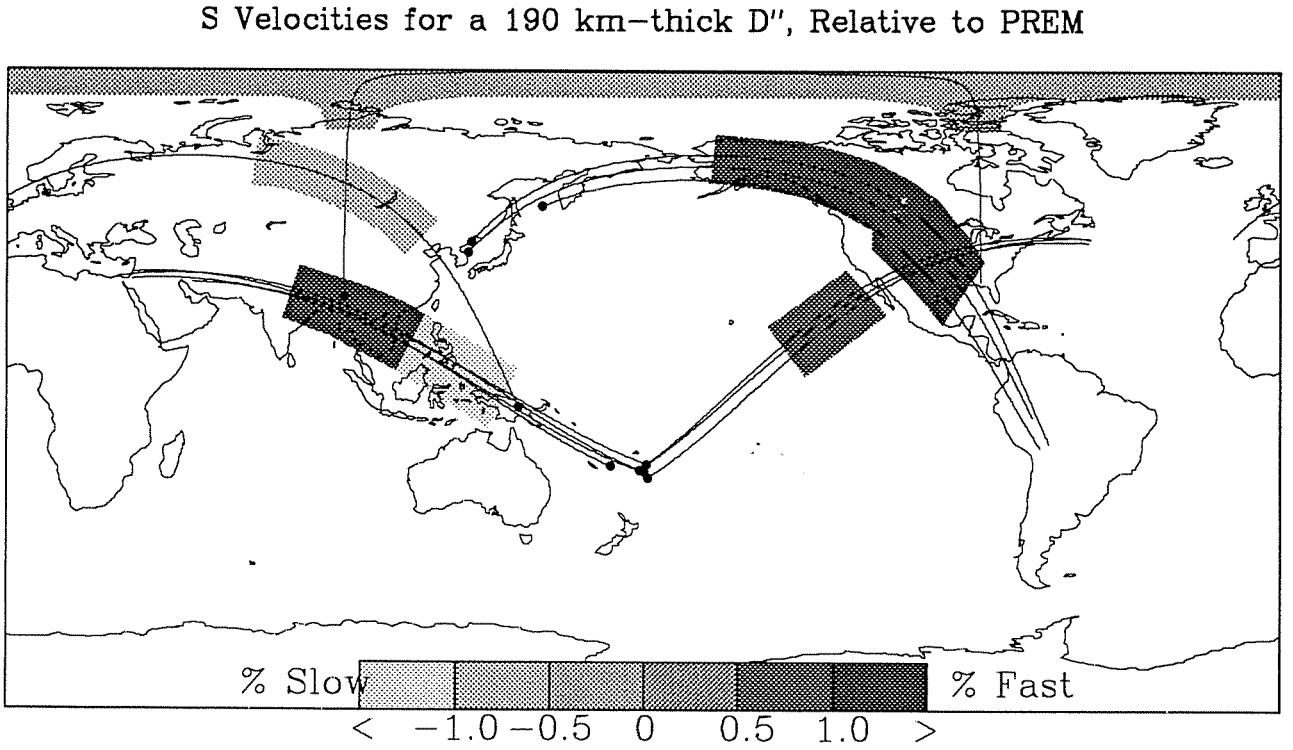

Fig. 7. Same as Figure 6, but for *S* velocities. Note that the shading scale is different from that in Figure 6.

TABLE 5. Velocity Results for Dual *P/S* Coverage, Including Poisson Ratios

Path Description	α_{190}, km/s	β_{190}, km/s	v
PREM	13.69	7.26	0.304
Taiwan/Japan to Western Americas	13.55	7.34	0.292
Indonesia to Europe	13.77	7.23	0.309
Tonga to North America	13.68	7.30	0.301
Tonga to Mid-East (first part)	13.25	7.04	0.303
Tonga to Mid-East (second part)	13.79	7.32	0.304

ScS precursor studies such as those of *Lay and Helmberger* [1983] and *Young and Lay* [1990] have found evidence of a very high *S* velocity zone and are also seen in the tomographic shear velocity models of *Tanimoto* [1987] and S. P. Grand (personal communication, 1991). The same high-velocity zone has not been seen there from *PcP* precursors, and in fact, tomographic *P* velocity models [*Morelli and Dziewonski*, 1987; *Inoue et al.*, 1990] also find slightly slower anomalies. While the diffracted waves have no resolution of the top of D", this type of discontinuous increase in shear velocity at the top of D" is a robust feature in several places along the CMB and is seen both from *ScS* precursors [*Young and Lay*, 1987; *Gaherty and Lay*, 1992] and the stacking of multiple-*ScS* phases [*Revenaugh and Jordan*, 1991].

The Poisson ratio varies in just the opposite way for the *Pd* and *Sd* profiles from Indonesia to Europe, which sample the CMB under north central Asia. Here the shear velocity is slow, while the *P* velocity is fast, and $v_{190} = 0.309$, which is almost 2% higher than for PREM. The only other location where we had both *P* and *S* coverage, as shown in Table 5, was under the eastern Pacific (from Tonga to North America), where the Poisson ratio, like that of the Tonga to Mid-East profiles, did not vary significantly from that of PREM.

Another region of the CMB that bore an interesting result was that under the northeastern Atlantic and Mediterranean seas. We only had *Pd* coverage, but all three profiles were noticeably slower than PREM, with $\Delta\alpha_{190} = -1.0\%$. It is interesting to note that the regionalized tomographic model of S. P. Grand (personal communication, 1991) for this region also shows a strong negative anomaly.

THERMOCHEMICAL MODELING

The quantification of lateral heterogeneity in D" is a necessary step in making determinations as to the physical properties of the rock at the base of the mantle. The changes in the shear and bulk moduli that we measured in the previous section can be viewed as the result of lateral changes in temperature and/or composition. The actual structure of D" probably involves a combination of chemical and thermal boundary layers [*Lay*, 1989] and is further complicated with phase changes, azimuthal anisotropy and lateral variations in D" thickness, much like the Earth's lithosphere. We attempt here a simple demonstration of the kind of effects lateral changes in temperature and composition would have on the D" velocity structure. While the type of results we find are nonunique and strongly limited by current knowledge of thermoelastic parameters of lower mantle materials, it gives a sense of the physical constraints on D" that a seismic model can give. It will also allow for a certain amount of discussion and speculation as to the nature of some of the seismic anomalies we have found, in particular, the great velocity low under Indonesia.

We use a third-order Birch-Murnaghan equation of state [*Birch*, 1952] in order to calculate seismic velocities at CMB conditions, starting with recent experimental values for the thermoelastic properties of the major lower mantle constituents. This technique is further discussed by *Bina and Silver* [1990], *Bina and Helffrich* [1992], and *Wysession* [1991], and here uses the iron and magnesium end members of perovskite and magnesiowüstite. While these ignore the perovskite structures of $CaSiO_3$ and Al_2O_3, they still account for nearly most of the lower mantle. The seismic velocities of these (Mg, Fe)SiO_3 and (Mg, Fe)O phases are calculated for D" conditions by starting with the elastic moduli and their derivatives and then making independent temperature and pressure corrections. The thermoelastic parameters used, which are extrapolated to standard temperature and pressure except where noted, are shown in Table 6 along with their sources. While these initial values are difficult to obtain experimentally and are therefore subject to change with future research, they will at least give us an order of magnitude understanding of the sensitivity of D" velocities to changes in temperature and composition. For any combination of minerals, the resulting velocities calculated for each are combined according to the molar proportions desired. We make the assumption that bulk material velocities vary linearly with the volume proportions of the minerals include, and that the partitioning coefficient between perovskite (*Pv*) and magnesiowüstite (*Mw*) is $K = 0.1$ [*Bell et al.*, 1979; *Ito and Yamada*, 1982].

We calculate the D " velocity variations that result for changes in three different parameters: temperature, Mg/Fe ratio, and Pv/Mw ratio. Because of uncertainties in the thermoelastic parameters, we present percentage variations in the velocities and not absolute values. Calculations are done for a pressure of 135 GPa and with an initial model of pyrolitic composition (Pv/(Pv+Mw) = 2/3) with a magnesium/metal ratio of 0.9 and a temperature of 3500 K. The velocity variations caused by deviations from this starting model are shown in Figures 8*a*-8*f*, which show the effects for *P* and *S* velocities separately. Figures 8*a*-8*f* are contour plots showing the two-parameter pairings of our three-parameter system, where contours are lines of equal velocity. The circle in each plot shows our initial model, and the heavy line through it is there-

TABLE 6. Thermoelastic Parameters Used for the Equation of State Velocity Calculations

Parameter	$MgSiO_3$	$FeSiO_3$	MgO	FeO
V_0	24.46[a]	25.49[a]	11.25[a]	12.25[a]
K_{S0}, GPa	268[b]	268[b]	163[a]	180[a]
K'_{S0}	4.0[b,c]	4.0[b,c]	4.1[a]	3.6[a]
δ_S	2.7[d]	2.7[d]	2.8[e]	3.0[f]
α_0[g] ($\times 10^{-5}$), K^{-1}	4.9[c]	4.9[c]	4.7[e]	5.9[e,a]
$d\alpha/dT$[h] ($\times 10^{-8}$), K^{-2}	1.7[c]	1.7[c]	1.04[e]	2.2[e,a]
$d\alpha/dT$[i] ($\times 10^{-8}$), K^{-2}	1.6[c]	1.6[c]	0.8[e]	1.7[e,a]
μ, GPa	185[j]	185[j]	132[e]	118[k]
μ'	1.9[j]	1.9[j]	2.5[l]	2.5[l]
$d\mu/dT$ ($\times 10^{-4}$), GPa/K	-3.3[j]	-3.3[j]	-2.5[e]	-2.5[e]

[a] *Jeanloz and Thompson* [1983].
[b] *Knittle and Jeanloz* [1987].
[c] *Mao et al.* [1991].
[d] *Bukowinski and Wolf* [1990].
[e] *Isaak et al.* [1989].
[f] *Sumino and Anderson* [1984].
[g] determined at 1300 K.
[h] linear value for $T < 1300$ K.
[i] linear value for $T > 1300$ K.
[j] *Yeganehi-Haeri et al.* [1989].
[k] *Jeanloz* [1990].
[l] *Agnon and Bukowinski* [1988].

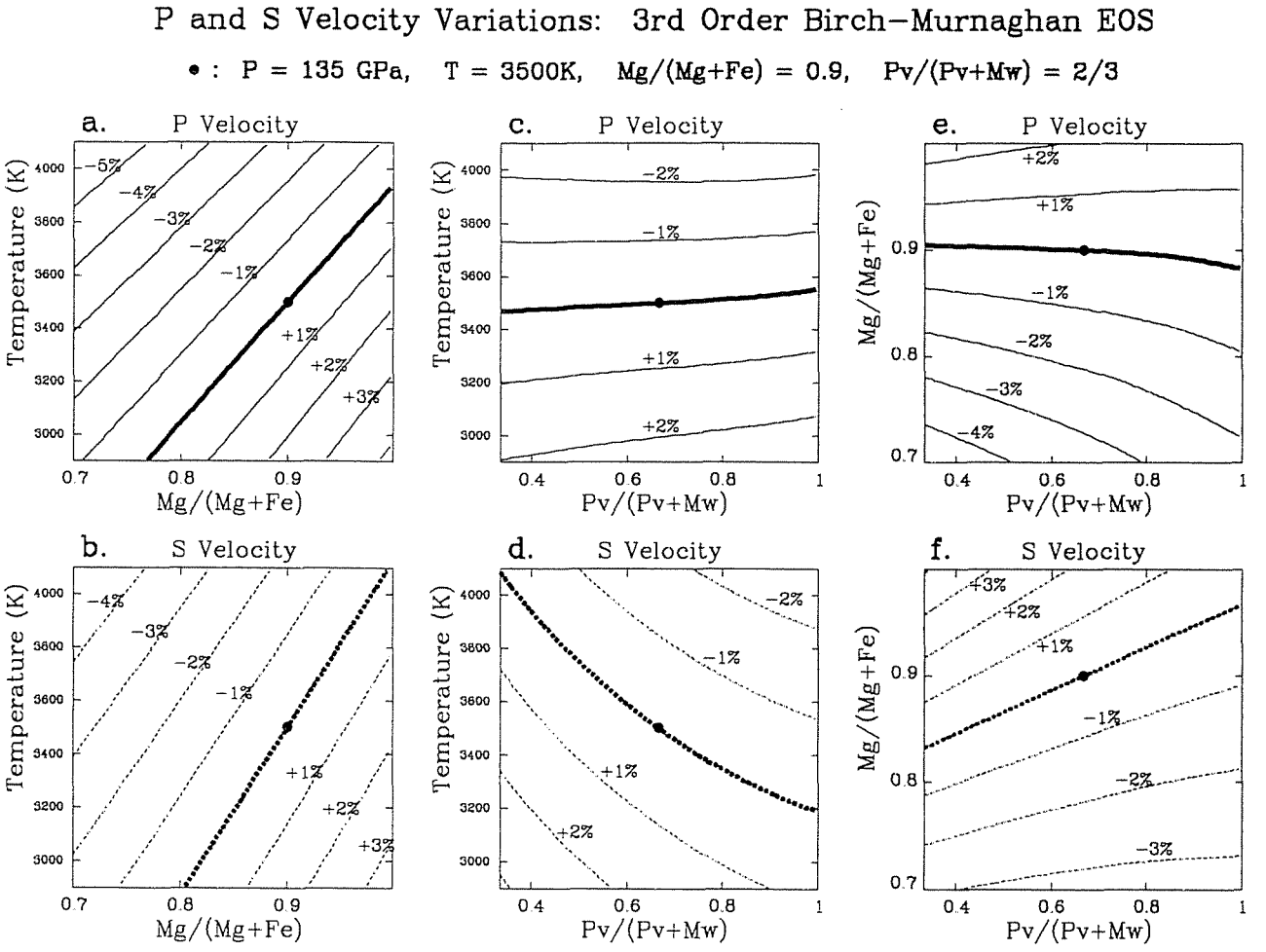

Fig. 8. Plots showing the variations in P and S velocities using a third-order Birch-Murnaghan equation of state and the experimental thermoelastic parameters listed in Table 6. Variations in three variables (temperature, Mg/Fe ratio, and silicate/oxide ratio) are shown relative to each other for P and S separately, with lines representing values of constant velocity in percent relative to the initial model. The circle in each diagram represents the initial model, which was at $P = 135$ GPa, $T = 3500$ K, Mg/(Mg+Fe) = 0.9, and Pv/(Pv+Mw) = 2/3 (Pv and Mw represent perovskite and magnesiowüstite). The lines through the circles are therefore lines of zero velocity variation. (a) P velocity for Mg/(Mg+Fe) versus temperature, (b) S velocity for Mg/(Mg+Fe) versus temperature, (a) P velocity for Pv/(Pv+Mw) versus temperature, (b) S velocity for Pv/(Pv+Mw) versus temperature, (a) P velocity for Pv/(Pv+Mw) versus Mg/(Mg+Fe), (b) S velocity for Pv/(Pv+Mw) versus Mg/(Mg+Fe).

fore the set of parameters that would give a velocity identical to it. Given the particular set of thermoelastic parameters we used, the seismic velocities were sensitive to both changes in temperatures and iron/magnesium ratios, though much less so for Pv/Mw deviations.

In Figures 8*a* and 8*b* we see that a 1% variation in seismic velocities could be explained by lateral variations of approximately 200° C for P and 300° C for S. The effect of changes in temperature on seismic velocities is most likely significantly less in D" than at the surface, because the temperature derivative of the thermal expansivity is much smaller [*Mao et al.*, 1991] and perovskite and magnesiowüstite seem stable and far from their solidi [*Knittle and Jeanloz*, 1989*a*, 1991; *Vassiliou and Ahrens*, 1982]. The seismic velocities are also very sensitive to the relative amounts of Fe and Mg: a little more than 5% variation from Mg/(Mg+Fe) = 0.90 would change P and S velocities by 1%. However, as shown in Figures 8*c* and 8*d*, the effects of deviations from a pyrolite composition are practically minimal. There is almost no effect on v_p, and an enormous change in Pv/(Pv+Mw) is required to elicit a significant change in v_s. Though Pv has much faster velocities than Mw at STP, recent estimates of the thermal expansion coefficient and derivatives of the elastic moduli predict this difference to decay with depth, thus making D" velocities less sensitive to Pv/Mw variations in this particular model [*Agnon and Bukowinski*, 1988; *Isaak et al.*, 1989; *Yeganeh-Haeri et al.*, 1989]. It is interesting, however, that for the case of Pv/Mw variations the Poisson ratio varies significantly, suggesting that in areas like the CMB under northern North America, where S velocities are fast but P velocities are slightly slow, this kind of variation may play a role. It is interesting to compare this experiment with the variations in temperature and Mg/Fe ratio: all three affect the P and S velocities at very different relative rates. With the ever clearer understanding of the temperature and pressure effects on the thermochemical properties of mantle rocks will eventually come the ability to determine in situ D" temperatures and compositions based on the absolute and relative P and S velocities determined thereof.

DISCUSSION

Most of the seismic variations from PREM for our profiles are of the order of approximately 1%, and if lateral variations in temperature over the top 200 km of the Earth are any indication of D" variations, then temperature could be a dominant factor driving the seismic heterogeneities there as well. Excluding the region under Indonesia, the ranges of anomalies from our averaged profiles correspond here to lateral $\Delta T \approx 400°$ C for P and $\Delta T \approx 500°$ C for S. These seem larger than one might reasonably allow, however, and we would expect other factors to be important.

The D" velocity low under Indonesia, more than 3% slow for both P and S velocities, certainly cannot be explained just as a thermal anomaly but would suggest an additional increase in iron. A very low Mg/(Mg+Fe) ratio of 0.7 would satisfy the Indonesian low, but we would not need this much iron if it was accompanied by an increase in temperature. This is demonstrated in Figure 9, where we see the P and S variations of Figures 8*a* and 8*b* superimposed, and the stippled region schematically represents the type of temperature and Mg/Fe variations that would satisfy the inferred D" average P and S velocities.

A possible geodynamic explanation that would account for both the slow velocities and the iron-temperature variations may involve coupling with core flow. There is a strong correlation between our D" velocities and the geomagnetically determined core flow model of *Voorhies* [1986] (and to a lesser extent, though still evident, of *Bloxham* [1989]). Our slow velocity region beneath Indonesia sits right over one of the largest regions of CMB core upwelling in the *Voorhies* [1986] models, as reproduced in Figure 10, and the adjacent fast velocities are above the largest *Voorhies* [1986] region of downwelling. Thermochemically, a reduction in D" seismic velocity would most likely be the result of increased temperature or iron content, and both of these would be expected

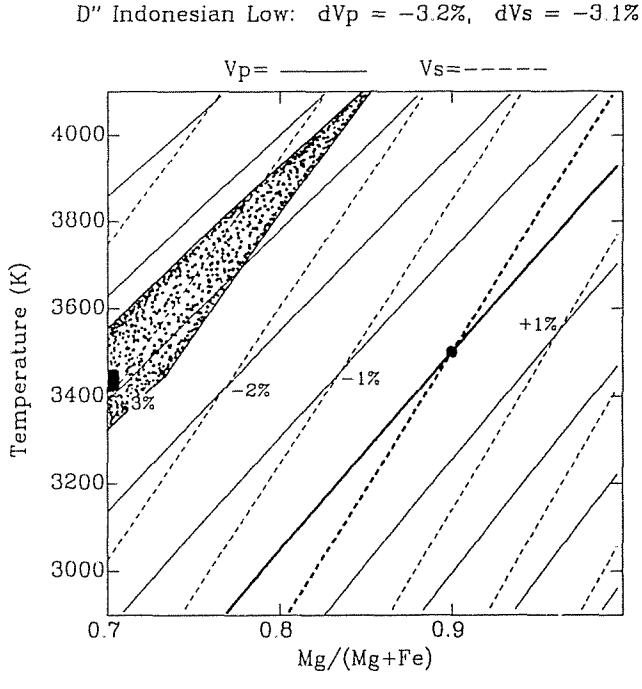

Fig. 9. A combination of Figures 8*a* and 8*b*, showing the combined variations in velocities due to temperature and metal content variations. The stippled area represents that part of the model that would adequately explain the 3% P and S velocity D" low-velocity anomalies under Indonesia.

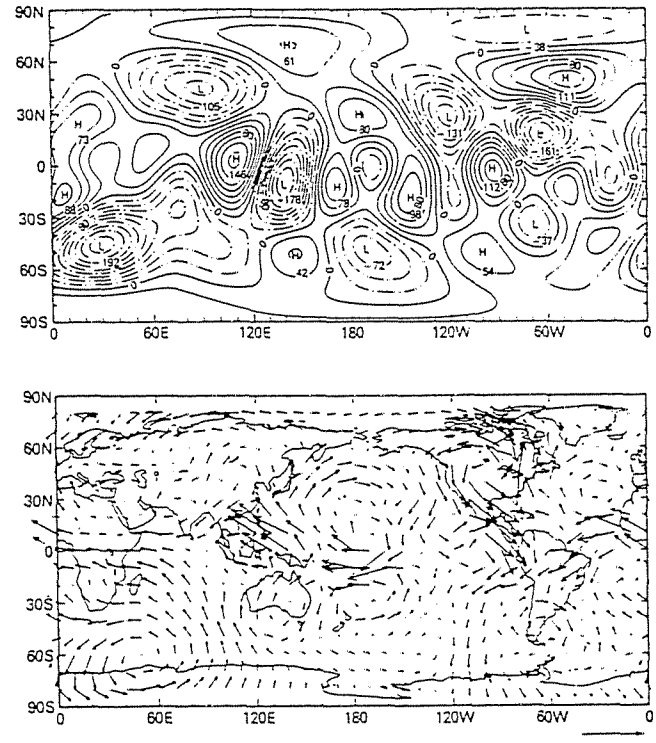

Fig. 10. (Top) Map of downwelling (surface convergence) at the top of the Earth's core (from Figure 6 of *Voorhies* [1986]). High's represent downwelling and lows are regions of upwelling, and units are in 10^{-4} yr^{-1}. The dramatic upwelling and downwelling centered at (0°N, 120°E) are at the same locations as the slow and fast parts of our Tonga to Mid-East CMB path. (Bottom) Horizontal core flow at the CMB for the period 1975-1980 (from Figure 10*c* of *Voorhies* [1986]). The reference vector, at the lower right, has a length of 87.125 km/yr. The flow from the upwelling to downwelling regions seen in the top figure is very evident.

above a core plume. *Knittle and Jeanloz* [1989*b*] proposed that reactions occur between the core liquid iron and the crystalline perovskite, with the resulting products of $MgSiO_3$, SiO_2 and the iron alloys FeO and FeSi [*Jeanloz*, 1990]. While the Mg-perovskite and stishovite will have faster than average velocities, the overall effect will be a decrease in velocity due to the presence of the metallic alloys. While the reaction should only occur directly at the CMB, it is very possible that the liquid iron seeps up into the mantle through capillary action [*Stevenson*, 1986], metaphorically parallel to the way water circulates through the crust. If this were the case, then we would expect there to be an increase in both heat flux and iron transport into the mantle above a region of vigorous core upwelling. Both would therefore be expected to contribute to the Indonesian D" velocity low.

There is, however, a difficulty in understanding why a correlation should exist between mantle and outer core features, when the core flow patterns are transitory in comparison to the longer times scales of mantle dynamics. Even though the core features under Indonesia and Southeast Asia have changed little over the last century and a half [*Bloxham and Jackson*, 1989], over much longer times scales we would require a dynamic coupling between the mantle and core to produce a significant mantle anomaly from core actions. Many of the studies of secular variation of core flow patterns do suggest the necessity of mantle-core coupling [*Bloxham*

and Gubbins, 1987]. This might take the form of either gravitational coupling between density inhomogeneities or topographic coupling due to the pressure gradients in the core near CMB topography, both of which are discussed by *Jault and LeMouël* [1989, 1990] and *Bloxham and Jackson* [1991].

Electromagnetic coupling between the mantle and core was suggested by *Jeanloz* [1990] as being due to lateral variations in D" electrical conductivity of more than 11 orders of magnitude. Metal-rich heterogeneities in D" would pin the magnetic field lines from the core, either distorting the image of flow patterns or controlling core flow near the CMB. The metal-rich D" rock needed to maintain this electromagnetic coupling could be the FeO and FeSi created from iron-silicate reactions and locally aggregated through intra-D" convective sweeping [*Davies and Gurnis*, 1986; *Zhang and Yuen*, 1988; *Hansen and Yuen*, 1989; *Sleep*, 1988] and would have significantly slower velocities than perovskite. Only small increased amounts of iron, in addition to a modest temperature increase, would be required to give us the slow D" velocities we see under Indonesia. So while the correlation between seismic and geomagnetic images may be coincidental, it is possible that this is an indication of significant coupling between the mantle and core. Further thermochemical modeling including the phases SiO_2 and FeSi will be required.

Another region of D" where we have strong enough diffracted wave coverage to make physical inferences is under the northern Pacific, sampled by Taiwan/Japan/Kurile earthquakes traveling to North American stations. The occurrence of fast shear velocities here would not be surprising in the case of full mantle convection. Subduction has been occurring for a long time here, and because the absolute plate motion of the North America/Pacific trench is very slow (of the order of 1 cm/yr [*Gripp and Gordon*, 1990]), there has been a lot of cold material that has been put into the mantle above where our diffracted waves sample the CMB. If the slabs penetrated into the lower mantle in the form of downgoing sheets, which are the favored mechanism of downgoing material transport in convection models such as those of *Olson et al.* [1990] and *Bercovici et al.* [1989], or if convection is limited to the upper mantle but is thermally coupled to the lower mantle, then we might expect to see an accumulation of the cold mantle dregs there at the CMB [*Ringwood*, 1975; *Hofman and White*, 1982]. The mantle shear velocity model of *Tanimoto* [1987] shows a ring of fast velocity extending all the way down to the CMB, and the averaged velocity anomaly of $\Delta\beta_{190} = +1.0\%$ that we find under the northern rim is certainly in keeping with this. Our equation of state calculations would require a 300°C decrease to model this, though this is higher than might be expected for downgoing material that has had a long time to attempt to thermally equilibrate with material around it.

This model is too simple, however, because it does not explain the presence of slow *P* velocities, which as mentioned earlier are seen in the *Pd* profiles and other seismic studies. What is required here is a mechanism that will describe the unusual change in the Poisson ratio: the concurrence of fast shear velocities with slow *P* velocities that have an averaged anomaly of $\Delta\alpha_{190} = -1.0\%$ relative to PREM. Such a circumstance does occur in our simplified thermochemical modeling, and in Figure 11 we show that the differing behaviors of the *P* and *S* velocities (which are superimposed) in response to temperature and silicate/oxide variations suggest particular conditions that are more favorable to it. The stippled region A of Figure 11 best satisfies our diffracted slownesses in this region, involving a temperature increase of ≈ 200°C and a large decrease in the amount of perovskite relative to magnesiowüstite. The stippled region B represents the seismic results for the *Pd* and

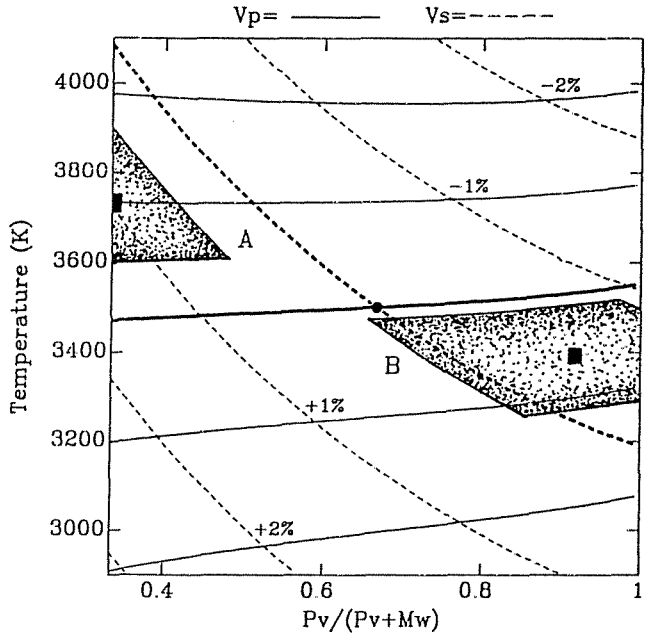

Fig. 11. A combination of Figures 8*c* and 8*d*, showing the combined variations in velocities due to temperature and silicate/oxide variations. Stippled area A represents that part of the plot that would satisfy the inferred average D" velocities under the rim of the North Pacific and North America, and stippled region B satisfies the velocities suggested by the diffracted profiles under north central Asia.

Sd profiles from Indonesia to Europe, which are the opposite case: slightly slow v_p and fast v_s. This part of D", under north central Asia, is modeled on the same plot by a decrease in temperature of 100°C and an increase of Pv/(Pv+Mw) to 0.9.

The other region of simultaneous *Pd* and *Sd* coverage is under the east central Pacific, from Tonga to North America, where we see velocities that do not differ significantly from PREM. There is a hint of fast velocities in the *Sd* slownesses ($\Delta\beta_{190} = +0.5\%$) which is possibly related to the same mechanism that causes the fast shear velocities seen to the north.

There were three *Pd* profiles from South and Central American earthquakes to Europe and Asia, sampling the CMB under the eastern North Atlantic and Mediterranean seas, which had a slow *P* anomaly averaging $\Delta\alpha_{190} = -1.0\%$. This would correspond, in Figure 8*a*, to an increase in temperature of 200°C, though we do not have and *Sd* profiles to help constrain it. There is some evidence to suggest that this could be a thermal anomaly, as the tomographic model of S. P. Grand (personal communication, 1991) shows slow shear velocity through much of the lower mantle in this region, and there are several active hotspots in this region including the Cape Verde, Canary, Azores, and New England [*Crough and Jurdy*, 1980]. If major hotspots are generated at the CMB, then we would expect to see a broad thickening of the mantle thermal boundary layer there, which should give rise to a long-wavelength seismic signal, such as is measured in the diffracted wave ray parameter. The Atlantic has the highest density of recognized hotspots, and it is very possible that the low velocities that are seen seismically in the lower mantle are a signature of this. If the relative amplitudes of the slow anomalies here and under Indonesia are significant, then this may be due to differences in the maturity of the hotspots. Many models of hotspot genesis show mushroomlike heads that rise up from the CMB and are followed by a thinner tail [*Olson et*

al., 1990; *Duncan and Richards*, 1991]. The northeastern Atlantic hotspots are mature, and we might expect less of a remnant D" feature, whereas there is no sign at the surface of an Indonesian hotspot [*Crough and Jurdy*, 1980], and we may be seeing the birth of one in the very slow velocities at the CMB there.

We do not suggest that the dynamics of a complicated thermochemical boundary layer can be constrained by modeling long-wavelength seismic waves with a three-parameter thermochemical model. There are many additional factors that are important. The comparisons drawn here are highly speculative, and the correlations may change as future experimental work is done. But both seismic and high-pressure mineral physics techniques are advancing rapidly and soon may be able to give definite answers as to the details of the CMB and its role in core and mantle convection. The combination of seismic and thermochemical modeling will continue to play a central role in the understanding of the coupling between the Earth's core and mantle.

CONCLUSIONS

An analysis of profiles of diffracted *P* and *S* waves has allowed for a limited mapping of the lateral heterogeneity of seismic velocities in D". Apparent ray parameters are determined for these linear profiles using the arrival times of the diffracted rays, modeled with reflectivity synthetic seismograms. The apparent slownesses are converted into mean D" velocities that are averaged for the bottom 190 km of the mantle according to the empirical relationships of *Mula and Müller* [1980]. The resulting inferred velocities suggest lateral variations of 4% for both *P* and *S*.

These values are strongly affected by one particular region of very slow velocities, at the CMB from beneath Indonesia from New Guinea to the South China Sea. This region at the CMB had inferred velocities, assuming a 190-km-thick D", that were 3% slower than for PREM. This was augmented by the proximity to a region of fast velocities underneath Southeast Asia. There is an interesting strong correlation between these velocities and core flow models determined from geomagnetics, especially that of *Voorhies* [1986]. The slow D" region sits right above a vigorous rising core plume, which if held in place over time because of electromagnetic coupling could be causing an increased influx of iron and heat into the mantle. Thermochemical modeling shows that a range of combinations of increased temperature and Fe/Me ratio would satisfy the low velocity anomaly. Such a region may represent the birth of a mantle hotspot.

Shear velocities 1% faster than PREM were found under North America and the northern rim of the Pacific Basin, consistent with *ScS* precursor studies such as that of *Young and Lay* [1990], but this region also had *P* velocities 1% slower than PREM, suggesting that a simple thermal anomaly may not be sufficient to explain it. This change in the Poisson ratio of 4% from that of PREM requires a chemical variation that affects *P* and *S* velocities very differently, and an example is shown where variations in the silicate/oxide ratio (in tandem with slight temperature changes) could satisfy this. There were also well-sampled regions, such as under the east central Pacific (from Tonga to North American stations), that were very adequately represented by the PREM velocities for D".

Acknowledgments. We would like to thank Andrea Morelli, Toshiro Tanimoto, and John Woodhouse for the use of their respective tomographic mantle models and Tim Clarke for presenting to us the reflectivity method. We thank Justin Revenaugh and Chris Young for their thoughtful and very helpful reviews. Thanks are expressed to Marge Yamasaki and Willie Lee for assistance in obtaining WWSSN records. We also thank Stephen Grand, Raymond Jeanloz, Elise Knittle, Thorne Lay, Colin Thomson, and Mark Woods for their helpful comments along the way. This research was partially supported by NSF grant EAR-84-05040.

REFERENCES

Agnon, A., and M. S. T. Bukowinski, High pressure shear moduli--A many-body model for oxides, *Geophys. Res. Lett., 15*, 209-212, 1988.

Alexander, S. S., and R. A. Phinney, A study of the core-mantle boundary using *P* waves diffracted by the earth's core, *J. Geophys. Res., 71*, 5943-5958, 1966.

Båth, M., Travel times of diffracted *P* waves, *Rep. 2-86*, Seismol. Dep., Uppsala Univ., Uppsala, 1986.

Bell, P. M., T. Yagi, and H.-K. Mao, Iron-magnesium distribution coefficients between spinel [$(Mg,Fe)_2SiO_4$], magnesiowüstite [(Mg,Fe)O], and perovskite [$(Mg,Fe)SiO_3$], Year Book Carnegie Inst. Washington, *78*, 618-621, 1979.

Berckhemer, H., and K. H. Jacob, Investigation of the dynamical process in earthquake foci by analyzing the pulse shape of body waves, *final report, contract AF61(052)-801*, 85 pp., Inst. of Meteorology and Geophys., Univ. of Frankfurt, 1968.

Bercovici, D., G. Schubert, and G. A. Glatzmaier, Influence of heating mode on three-dimensional mantle convection, *Geophys. Res. Lett., 16*, 617-620, 1989.

Bina, C. R., and G. R. Helffrich, Calculation of elastic properties from thermodynamic equation of state principles, *Ann. Rev. Earth Planet. Sci.*, in press, 1992.

Bina, C. R., and P. G. Silver, Constraints on lower mantle composition and temperature from density and bulk sound velocity profiles, *Geophys. Res. Lett., 17*, 1153-1156, 1990.

Birch, F., Elasticity and constitution of the Earth's interior, *J. Geophys. Res., 57*, 227-286, 1952.

Bloxham, J., Simple models of fluid flow at the core surface derived from geomagnetic field models, *Geophys. J. Int., 99*, 173-182, 1989.

Bloxham, J., and D. Gubbins, Thermal core-mantle interactions, *Nature, 325*, 511-513, 1987.

Bloxham, J., and A. Jackson, Simultaneous stochastic inversion for geomagnetic main field and secular variation, 2, 1820-1980, *J. Geophys. Res., 94*, 15,753-15,769, 1989.

Bloxham, J., and A. Jackson, Fluid flow near the surface of Earth's outer core, *Rev. Geophys., 29*, 97-120, 1991.

Bolt, B. A., *PdP* and *PKiKP* waves and diffracted *PcP* waves, *Geophys. J. R. Astron. Soc., 20*, 367-382, 1970.

Bolt, B. A., and M. Niazi, *S* velocities in D" from diffracted *SH*-waves at the core boundary, *Geophys. J. R. Astron. Soc., 79*, 825-834, 1984.

Bolt, B. A., M. Niazi, and M. R. Somerville, Diffracted *ScS* and shear velocity at the core boundary, *Geophys. J. R. Astron. Soc., 19*, 299-305, 1970.

Bukowinski, M. S. T., and G. H. Wolf, Thermodynamically consistent decompression: Implications for lower mantle composition, *J. Geophys. Res., 95*, 12,583-12,593, 1990.

Bullen, K. E., Compressibility-pressure hypothesis and the Earth's interior, *Mon. Not. R. Astron. Soc., Geophys. Suppl., 5*, 355-368, 1949.

Chandra, U., The Peru-Bolivia border earthquake of August 15, 1963, *Bull. Seismol. Soc. Am., 60*, 639-646, 1970.

Chapman, C. H., and R. A. Phinney, Diffracted seismic signals and their numerical solution, *Methods Comput. Phys., 12*, 165-230, 1972.

Choy, G. L., Theoretical seismograms of core phases calculated by frequency-dependent full wave theory, and their interpretation, *Geophys. J. R. Astron. Soc., 51*, 275-312, 1977.

Cleary, J., The *S* velocity at the core-mantle boundary, from observations of diffracted *S*, *Bull. Seismol. Soc. Am., 59*, 1399-1405, 1969.

Cormier, V. F., Slab diffraction of *S* waves, *J. Geophys. Res., 94*, 3006-3024, 1989.

Crough, S. T., and D. M. Jurdy, Subducted lithosphere, hotspots, and the geoid, *Earth Planet. Sci. Lett., 48*, 15-22, 1980.

Davies, G. F., and M. Gurnis, Interaction of mantle dregs with convection: lateral heterogeneity at the core-mantle boundary, *Geophys. Res. Lett., 13*, 1517-1520, 1986.

Denham, D., Summary of earthquake focal mechanisms for the Western Pacific-Indonesian region, 1929-1973, *Rep. SE-3, World Data Cent. A for Solid Earth Geophys.*, Boulder, Colo., 1977.

Doornbos, D. J., and J. C. Mondt, Attenuation of *P* and *S* waves diffracted around the core, *Geophys. J. R. Astron. Soc., 57*, 353-379, 1979*a*.

Doornbos, D. J., and J. C. Mondt, *P* and *S* waves diffracted around the core and the velocity structure at the base of the mantle, *Geophys. J. R. Astron. Soc., 57*, 381-395, 1979*b*.

Duncan, R. A., and M. A. Richards, Hotspots, mantle plumes, flood basalts, and true polar wander, *Rev. Geophys., 29*, 31-50, 1991.

Dziewonski, A. M., and D. L. Anderson, Preliminary reference Earth model, *Phys. Earth Planet. Inter., 25*, 297-356, 1981.

Dziewonski, A. M., and D. L. Anderson, Travel times and station corrections for *P* waves at teleseismic distances, *J. Geophys. Res., 88*, 3295-3314, 1983.

Espinoza, A. F., *P* in the shadow zone of Earth's core, part 1, *Pure Appl. Geophys., 67*, 5-14, 1967.

Fitch, T. J., Earthquake mechanisms and island arc tectonics in the Indonesian-Philippine region, *Bull. Seismol. Soc. Am., 60*, 565-591, 1970.

Fitch, T. J., and P. Molnar, Focal mechanisms along inclined earthquake zones in the Indonesian-Philippine region, *J. Geophys. Res., 75*, 1431-1444, 1970.

Gaherty, J. B., and T. Lay, Investigation of laterally heterogeneous shear velocity structure in D" beneath Eurasia, *J. Geophys. Res., 97*, 417-435, 1992.

Giardini, D., Systematic analysis of deep seismicity: 200 centroid-moment tensor solutions to earthquakes between 1977 and 1980, *Geophys. J. R. Astron. Soc., 77*, 883-911, 1984.

Gripp, A. E., and R. G. Gordon, Current plate velocities relative to the hotspots incorporating the NUVEL-1 global plate motion model, *Geophys. Res. Lett., 17*, 1109-1112, 1990.

Hales, A. L., and J. L. Roberts, Shear velocities in the lower mantle and the radius of the core, *Bull. Seismol. Soc. Am., 60*, 1427-1436, 1970.

Hansen, U., and D. A. Yuen, Dynamical influences from thermal-chemical instabilities at the core-mantle boundary, *Geophys. Res. Lett., 16*, 629-632, 1989.

Hofman, A. W., and W. M. White, Mantle plumes from ancient oceanic crust, *Earth Planet. Sci. Lett., 57*, 421-436, 1982.

Inoue, H., Y. Fukao, K. Tanabe, and Y. Ogata, Whole mantle *P*-wave travel time tomography, *Phys. Earth Planet. Inter., 59*, 294-328, 1990.

Isaak, D. G., O. L. Anderson, and T. Goto, Measured elastic moduli of single-crystal MgO up to 1800 K, *Phys. Chem. Miner., 16*, 704-713, 1989.

Isacks, B., and P. Molnar, Distribution of stresses in the descending lithosphere from a global survey of focal-mechanism solutions of mantle earthquakes, *Rev. Geophys., 9*, 103-174, 1971.

Ito, E., and H. Yamada, Stability relations of silicate spinels, ilmenites and perovskites, in *High-Pressure Research in Geophysics*, edited by S. Akimoto and M. H. Manghnani, pp. 405-419, Center for Academic Publishing, Tokyo, 1982.

Jault, D., and J.-L. LeMouël, The topographic torque associated with a tangentially geostrophic motion at the core surface and inferences on the flow inside the core, *Geophys. Astrophys. Fluid Dyn., 48*, 273-296, 1989.

Jault, D., and J.-L. LeMouël, Core-mantle boundary shape: Constraints inferred from the pressure torque acting between the core and mantle, *Geophys. J. Int., 101*, 233-241, 1990.

Jeanloz, R., The nature of the Earth's core, *Annu. Rev. Earth Planet. Sci., 18*, 357-386, 1990.

Jeanloz, R., and A. B. Thompson, Phase transitions and mantle discontinuities, *Rev. Geophys., 21*, 51-74, 1983.

Jeffreys, H., and K. E. Bullen, Seismological tables, 50 pp., Brit. Assoc. for the Adv. Science, London, 1970.

Johnson, T., and P. Molnar, Focal mechanisms and plate tectonics of the Southwest Pacific, *J. Geophys. Res., 77*, 5000-5032, 1972.

Kanamori, H., and G. S. Stewart, Mode of the strain release along the Gibbs Fracture Zone, Mid-Atlantic Ridge, *Phys. Earth Planet. Inter., 11*, 312-332, 1976.

Katsumata, M., and L. R. Sykes, Seismicity and tectonics of the western Pacific: Izu-Mariana-Caroline and Ryukyu-Taiwan regions, *J. Geophys. Res., 74*, 5923-5948, 1969.

Knittle, E., and R. Jeanloz, Synthesis and equation of state of (Mg, Fe)SiO_3 perovskite to over 100 GPa, *Science, 235*, 668-670, 1987.

Knittle, E., and R. Jeanloz, Melting curve of (Mg,Fe)SiO_3 perovskite to 96 GPa: Evidence for a structural transition in lower mantle melts, *Geophys. Res. Lett., 16*, 421-424, 1989*a*.

Knittle, E., and R. Jeanloz, Simulating the core-mantle boundary: an experimental study of high-pressure reactions between silicates and liquid iron, *Geophys. Res. Lett., 16*, 609-612, 1989*b*.

Knittle, E., and R. Jeanloz, The high pressure phase diagram of $Fe_{0.94}O$: A possible constituent of the Earth's core, *J. Geophys. Res., 96*, 16,169-16,180, 1991.

Lay, T., Structure of the core-mantle transition zone: A chemical and thermal boundary layer, *Eos Trans. AGU, 70*, 49, 1989.

Lay, T., and D. V. Helmberger, A lower mantle *S*-wave triplication and the velocity structure of D", *Geophys. J. R. Astron. Soc., 75*, 799-837, 1983.

Mao, H. K., R. J. Hemley, Y. Fei, J. F. Shu, L. C. Chen, A. P. Jephcoat, Y. Wu, and W. A. Bassett, Effect of pressure, temperature and composition on lattice parameters and density of (Fe,Mg)SiO_3-perovskites to 30 GPa, *J. Geophys. Res., 96*, 8069-8079, 1991.

Mondt, J. C., *SH* waves: Theory and observations for epicentral distances greater than 90 degrees, *Phys. Earth Planet. Inter., 15*, 46-59, 1977.

Morelli, A., and A. M. Dziewonski, Topography of the core-mantle boundary and lateral heterogeneity of the liquid core, *Nature, 325*, 678, 1987.

Mula, A. H., Amplitudes of diffracted long-period *P* and *S* waves and the velocities and *Q* structure at the base of the mantle, *J. Geophys. Res., 86*, 4999-5011, 1981.

Mula, A. H., and G. Müller, Ray parameters of diffracted long pe-

riod *P* and *S* waves and the velocities at the base of the mantle, *Pure Appl. Geophys., 118*, 1270-1290, 1980.

Okal, E. A., and R. J. Geller, Shear-wave velocity at the base of the mantle from profiles of diffracted *SH* waves, *Bull. Seismol. Soc. Am., 69*, 1039-1053, 1979.

Olson, P., P. G. Silver, and R. W. Carlson, The large-scale structure of convection in the Earth's mantle, *Nature, 344*, 209-215, 1990.

Revenaugh, J., and T. H. Jordan, Mantle layering from *ScS* Reverberations, 4, The lower mantle and core-mantle boundary, *J. Geophys. Res., 96*, 19,811-19,824, 1991.

Ringwood, A., *Composition and Petrology of the Earth's Mantle*, McGraw-Hill, New York, 1975.

Sacks, I. S., Diffracted *P* wave studies of the Earth's core, 2, Lower mantle velocity, core size, lower mantle structure, *J. Geophys. Res., 72*, 2589-2594, 1967.

Sleep, N. H., Gradual entrainment of a chemical layer at the base of the mantle by overlying convection, *Geophys. J. R. Astron. Soc., 95*, 437-447, 1988.

Stevenson, D. J., On the role of surface tension in the migration of melts and fluids, *Geophys. Res. Lett., 13*, 1149-1152, 1986.

Sumino, Y., and O. L. Anderson, Elastic constants of minerals, in *CRC Handbook of Physical Properties of Rocks*, Volume III, edited by R. S. Carmichael, pp. 39-138, CRC Press, Boca Raton, Fla., 1984.

Tandon, A. N., and H. N. Srivastava, Fault plane solutions as related to known geological faults in and near India, *Ann. Geofis., 28*, 13-27, 1975.

Tanimoto, T., The three-dimensional shear wave structure in the mantle by overtone waveform inversion, I, Radial seismogram inversion, *Geophys. J. R. Astron. Soc., 89*, 713-740, 1987.

Vassiliou, M. S., and T. J. Ahrens, The equation of state of $Mg_{0.6}Fe_{0.4}O$ to 200 GPa, *Geophys. Res. Lett., 9*, 127-130, 1982.

Vinnik, L. P., V. Farra, and B. Romanowicz, Observational evidence for diffracted *SV* in the shadow of the Earth's core, *Geophys. Res. Lett., 16*, 519-522, 1989.

Voorhies, C. V., Steady flows at the top of Earth's core derived from geomagnetic field models, *J. Geophys. Res., 91*, 12,444-12,466, 1986.

Woodhouse, J. H., and A. M. Dziewonski, Models of the upper and lower mantle from waveforms of mantle waves and body waves, *Eos Trans. AGU, 68*, 356-357, 1987.

Wysession, M. E., Diffracted seismic waves and the dynamics of the core-mantle boundary, Ph.D. thesis, 190 pp., Northwest. Univ., Evanston, Ill., 1991.

Wysession, M. E., and E. A. Okal, Evidence for lateral heterogeneity at the core-mantle boundary from the slowness of diffracted *S* profiles, in *Structure and Dynamics of Earth's Deep Interior, Geophys. Monogr. Ser.*, Vol. 46, edited by D. E. Smylie and R. Hide, pp. 55-63, AGU, Washington, D. C., 1988.

Wysession, M. E., and E. A. Okal, Regional analysis of D" velocities from the ray parameters of diffracted *P* profiles, *Geophys. Res. Lett., 16*, 1417-1420, 1989.

Yeganeh-Haeri, A., D. J. Weidner, and E. Ito, Elasticity of $MgSiO_3$ in the perovskite structure, *Science, 243*, 787-789, 1989.

Young, C. J., and T. Lay, The core mantle boundary, *Ann. Rev. Earth Planet. Sci., 15*, 25-46, 1987.

Young, C. J., and T. Lay, Multiple phase analysis of the shear velocity structure in the D" region beneath Alaska, *J. Geophys. Res., 95*, 17,385-17,402, 1990.

Zhang, S., and D. A. Yuen, Dynamical effects on the core-mantle boundary from depth-dependent thermodynamical properties of the lower mantle, *Geophys. Res. Lett., 15*, 451-454, 1988.

C. R. Bina and E. A. Okal, Department of Geological Sciences, Northwestern University, Evanston, IL 60208.

M. E. Wysession, Department of Earth and Planetary Sciences, Washington University, Campus Box 1169, One Brookings Dr., St. Louis, MO 63130-4899.

(Received October 15, 1991;
revised February 14, 1992;
accepted February 25, 1992.)